Effect of fibrous capsule formation on doxorubicin distribution in radiofrequency ablated rat livers

Elvin Blanco,[1] Feng Qian,[1] Brent Weinberg,[1] Nicholas Stowe,[2] James M. Anderson,[3] Jinming Gao[1]
[1]*Department of Biomedical Engineering, Case Western Reserve University, Cleveland, Ohio 44106*
[2]*Department of Surgery, School of Medicine, Case Western Reserve University, Cleveland, Ohio 44106*
[3]*Institute of Pathology, University Hospitals of Cleveland, Cleveland, Ohio 44106*

Received 24 October 2003; accepted 16 December 2003
Published online 22 March 2004 in Wiley InterScience (www.interscience.wiley.com). DOI: 10.1002/jbm.a.30001

Abstract: In this study, we report the histological findings of a combined therapy using radiofrequency ablation and intratumoral drug delivery in rat livers, with special attention to wound-healing processes and their effects on drug transport in post-ablated tissue. Doxorubicin-loaded millirods were implanted in rat livers that had undergone medial lobe ablation. Millirods and liver samples were retrieved upon animal sacrifice at time points ranging from 1 h to 8 days. Results demonstrate a clearly defined area of coagulative necrosis within the ablation boundary. The wound-healing response, complete with the appearance of inflammatory cells, neovascularization, and the formation of a fibrous capsule, was also observed. At the 8-day time point, fluorescence imaging analysis showed a higher concentration of doxorubicin localized within the ablation region, with its distribution hampered primarily by fibrous capsule formation at the boundary. Given the variant nature of ablated liver, a mathematical model devised previously by our laboratory describes the data well up to 4 days, but loses reliability at 8 days. These results provide useful mechanistic insights into the wound-healing response after radiofrequency ablation and polymer millirod implantation, as well as the impact this natural corollary has on drug distribution.
 J Biomed Mater Res 69A: 398–406, 2004

Key words: radiofrequency ablation; doxorubicin transport; wound-healing response; intratumoral drug delivery; polymer implants

INTRODUCTION

Although surgical excision remains the most curable option in treating hepatic cancer, only a handful of liver cancer patients are candidates for resection. Presently, several obstacles including anatomical inaccessibility of the tumor and the coexistence of various tumor nodule sites have led to a burgeoning focus on less invasive and more patient-compliant treatment modalities such as cryotherapy,[1–3] high-intensity focused ultrasound,[4] and radiofrequency (RF) ablation.[5–8] The latter technique, which utilizes heat supplied by a needle electrode to eliminate tumors, has proven effective in destroying cancerous cells within the heat burst radius, but fails to eliminate remnant and viable malignant cells found at the periphery of ablation.[9–11] In an attempt to improve this technical shortcoming, our research laboratory proposes a combination therapy consisting of the following: 1) image-guided RF ablation of solid tumors, followed by 2) the implantation of a polymer millirod drug delivery device, which permits intratumoral delivery of doxorubicin, an anticancer drug, so as to eradicate any residual cancer cells.[12–16] Hence, vital to the efficacy of the aforementioned combined strategy is the knowledge that RF ablation can drastically alter the liver tissue environment, potentially modifying the means of drug transport from the millirod implant to the surrounding liver parenchyma.

Fortunately, many recent studies have been devoted to the advancement and the establishment of RF ablation as a promising application for cancer therapy. As a result of the intense research and practice over the years, it is now well known that RF ablation causes coagulative necrosis of tissue because of the local parenchyma surpassing temperatures of up to 100°C. Destruction of tissue microvasculature accompanies the phenomenon, and peripheral small-diameter venules become thrombotic. The consequential burn wound produced by RF ablation elicits a wound-healing response from the host, brought about by the release of inflammatory mediators. Although the

Correspondence to: J. Gao; e-mail: jinming@case.edu
Contract grant sponsor: National Institutes of Health; contract grant number: R01-CA-90696

pathophysiology of the inflammatory response caused by physical injury, burns, and the implantation of foreign materials in the body has been extensively documented,[17–20] to the best of our knowledge, the wound-healing response in liver tissues after RF ablation and its effect on drug distribution has not been reported.

Previous research conducted by our laboratory has led to the rational design of dose formulations, characterization of drug distribution, and mathematical modeling of transport within the ablated liver tissue environment.[13,15] The mathematical model in its present form assumes that drug diffusivities and drug elimination coefficients remain constant throughout the duration of the polymer millirod implantation, as the environment is considered time-invariant. Although the model does provide acceptable approximations up to 4 days after implantation,[15] the effect of the wound-healing response on drug transport at later times has not been fully examined.

The objective of this work is to histologically monitor the wound-healing response in ablated and nonablated liver tissue with implanted polymer millirods over an 8-day period of time. We hypothesize that structural changes resulting from wound healing, especially fibrous capsule formation, will greatly affect the drug transport properties *in vivo*. Such structural changes need to be taken into consideration for the future design of polymer millirods for liver cancer treatment.

MATERIALS AND METHODS

Materials

Poly(D,L-lactide) (PLA, inherent viscosity 0.67dL/g) and poly(D,L-lactide-*co*-glycolide) (PLGA, lactide/glycolide = 1:1, MW 50,000 Da, inherent viscosity 0.65 dL/g) were purchased from Birmingham Polymers, Inc. (Birmingham, AL). Poly(ethylene glycol) (PEG, M_n 4600 Da) was obtained from Aldrich (Milwaukee, WI). Doxorubicin HCl solution was purchased from Bedford Laboratories (Bedford, OH). Tris-buffered saline solution (1X) was purchased from Fisher Scientific (Pittsburgh, PA).

Animals

Male Sprague-Dawley rats (350–450 g) were obtained from Charles River Laboratories (Boston, MA). Animal procedures were adhered to the National Institutes of Health Guidelines and an approved protocol by the Institutional Animal Care and Use Committee at Case Western Reserve University.

Fabrication and *in vitro* characterization of sustained-release millirods

The doxorubicin HCl solution was desalted by dialysis in distilled water. The purified doxorubicin solution was then lyophilized to provide a fine powder. Monolithic PLGA millirods containing 5% doxorubicin, 25% NaCl, and 70% PLGA were fabricated by a compression-heat molding procedure.[12] The cylindrical millirods, measuring 1.6 mm in diameter, were cut to a length of 8 mm.

Sustained-release millirods were fabricated following a published procedure.[16] First, the monolithic PLGA millirods were dipped into PEG/PLA solution in CH_2Cl_2. The total polymer concentration was 200 mg/mL and the PEG in PLA percentage was 10%. The dipping speed was controlled by a vertically placed syringe pump at 2 mm/s. The millirods were then air-dried for 24 h followed by another round of dip-coating at the alternate end. The resulting membrane-encased millirods provide a total sustained-release phase of doxorubicin over 7 days at approximately 0.4 mg/(day · cm millirod) in Tris buffer (pH 7.4, 37°C).[16]

RF ablation and millirod implantation

Male Sprague-Dawley rats were anesthetized with an intraperitoneal injection of sodium pentobarbital (50 mg/kg). The abdomen was shaved and prepped with Betadine and alcohol. A local anesthetic, Marcaine, was injected subcutaneously just before skin incision. The medial lobe of the liver was then exposed through a small midline incision and exteriorized for RF ablation and millirod placement. Liver tissue ablation was produced using RF-generated current (0.09–0.12 A) from a 19-gauge needle electrode (Radionics®, Burlington, MA) at 90° ± 2° C for a duration of 2 min. The ablated region extended approximately 4–5 mm from the electrode source. After the removal of the electrode, a millirod was inserted within the electrode tract and a small piece of cotton was sewn at the top. After the ablation procedure, 5 mL of saline solution was poured into the abdomen to assist in animal recovery, and the abdomen was then sutured. The animals were kept alive for predetermined periods of 1, 4, and 7 h, as well as 1, 2, 4, 6, and 8 days, with retrieval of polymer millirods occurring after animal sacrifice. The liver was recovered and cut perpendicular to the long axis of millirod implantation. Half was fixed in 10% formalin solution for future histological analysis, whereas the other half was preserved for doxorubicin concentration analysis.

Histology and fluorescence imaging analysis

After fixation in 10% formalin solution, the liver samples for histology analysis were embedded in paraffin, sliced to a thickness of 5 μm, and stained with hematoxylin and eosin (H&E) and Masson's trichrome (MTC) stains. Histology images were taken using a Nikon Eclipse (TE300 model) microscope.

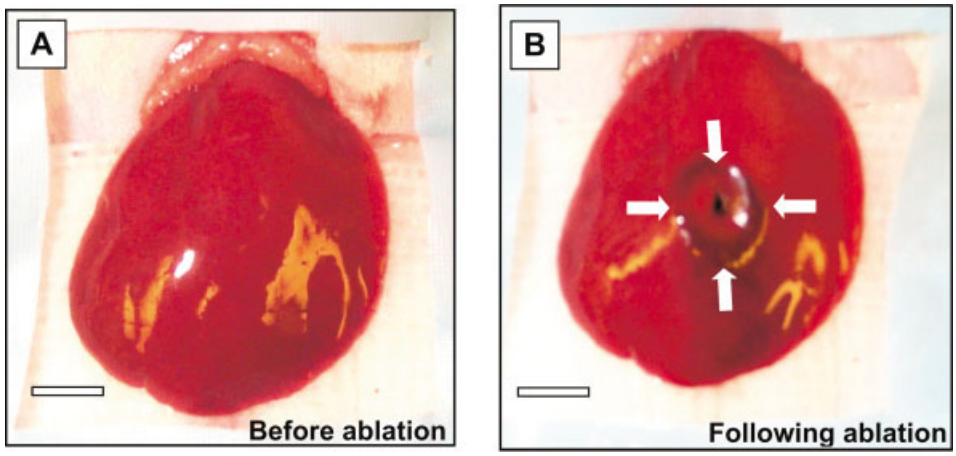

Figure 1. Medial lobe of rat liver before and immediately after RF ablation. The arrows point to the hemorrhagic rim formed as a result of ablation. The scale bars represent 5 mm. [Color figure can be viewed in the online issue, which is available at www.interscience.wiley.com.]

Frozen liver samples set aside for fluorescence microscopy analysis were mounted on a cryostat microtome with O.C.T. embedding medium (Miles Inc., Elkhart, IN), sectioned at −15°C to a thickness of 100 μm, and placed on a glass slide. Given that doxorubicin is a fluorescent molecule with excitation and emission wavelengths of 488 and 580 nm, respectively, the fluorescence microscopy images were captured using a rhodamine filter on the Nikon Eclipse microscope. For quantitative fluorescence imaging studies, the liver slices were scanned using a fluorescence imager (FluoroImager™ SI model; Molecular Dynamics, Sunnyvale, CA). Fluorescence images were saved in TIFF format and fluorescence intensity in the images was converted to drug concentration using MatLab software (version 5.3) and a previously determined calibration curve.[15] Image J software (provided free of charge by the National Institutes of Health) was used to calculate the doxorubicin concentrations spanning radially outward from the millirod implantation site. The concentration–distance profiles were then averaged from eight radial directions, with an approximate separation of 45° between each direction.

RESULTS

Gross and histological analysis of liver samples

Gross examination of rat livers

Figure 1 compares the gross images of rat livers before and immediately after RF ablation of the medial lobe of a rat liver. As depicted in Figure 1(A), the medial lobe of the liver displays a glossy, smooth, and bright red external surface before ablation, characteristics indicative of a healthy liver. However, subsequent to ablation, the liver displays a pale circular region of tissue shrinkage surrounded by a hemorrhagic rim that delineates the radius of ablation, averaging 3–5 mm. The central cavity visible in Figure 1(B) corresponds to the ablation probe insertion site, serving furthermore as the site for millirod implantation.

One hour to 4 days after ablation

Within a matter of hours after RF ablation and millirod implantation, a clear distinction between ablated and nonablated zones becomes apparent in the liver samples. Figure 2(A) shows the immediate post-ablated environment, composed of a region within the radius of ablation akin to a coagulative, necrotic core—an area lacking well-defined sinusoidal and nuclear structure. The highly porous interstitial space owes itself mainly to tissue shrinkage during the charring process. The nonablated region, however, displays the characteristics of normal liver tissue morphology, including intact sinusoidal structure and undamaged hepatocytes with integral nuclear features. The results obtained are consistent with a previous short-term histological study of ablated rat livers.[15] Given the short time lapse after ablation, events characteristic of the acute inflammatory response cannot yet be discerned. Inflammatory cell migration, the initial stage of the acute wound-healing process, is well underway 2 days after RF ablation and millirod implantation. A clearly defined zone of inflammatory cells, predominantly neutrophils and monocytes, is present in Figure 2(B), and the cells are shown accumulating at the ablation boundary, separating the necrotic core from the nonablated region in the process. MTC-stained images at the 2-day mark (data not shown) do not illustrate any indication of collagen deposition by fibroblasts, and no fibrous capsule formation can be seen.

Four days after RF ablation, the inflammatory re-

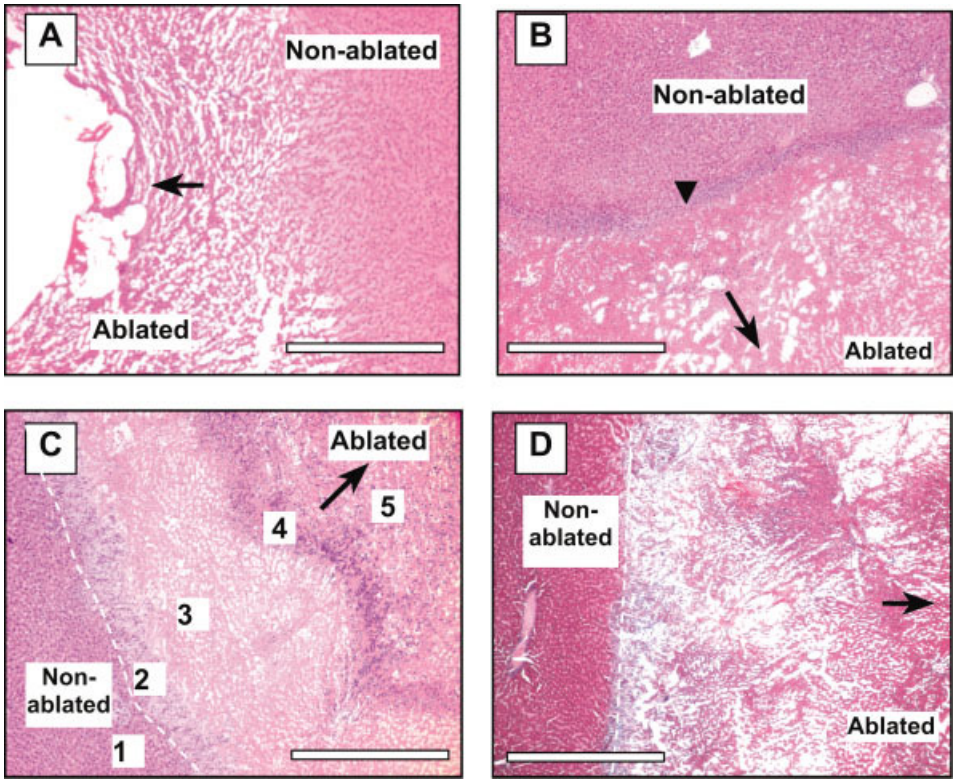

Figure 2. Histology analysis of liver samples 1 h, 2 and 4 days after RF ablation and millirod implantation. (A) One-hour H&E stained sample at original magnification of 4×. (B) Two-day H&E stained sample (original magnification 4×). The triangle in (B) points to the sharply defined zone of inflammatory cells at the ablation boundary. (C) and (D) H&E and MTC-stained samples, respectively, 4 days after RF ablation (original magnification 4×). Black arrows in all images point to the millirod implantation and ablation probe insertion site. The scale bars in all four images represents 1 mm. [Color figure can be viewed in the online issue, which is available at www.interscience.wiley.com.]

sponse has progressed and become quite extensive, yielding five distinct zones in the ablated and adjacent nonablated tissue, as is evident in Figure 2(C). The first zone consists of viable, nonablated hepatocytes, located well outside of the ablation radius. The second zone is characterized by fibroblast activity, whereas the third zone represents an area of cellular debris left behind by the migration of inflammatory cells, which in turn comprise the fourth zone. The fifth zone, and that closest to the ablation and millirod implantation site, represents the necrotic core.

Close observation of the distinct zones at higher magnifications yields insight into their various characteristics (data not shown). Analysis of the first zone at a higher magnification shows that this nonablated region is composed mainly of viable and healthy hepatocytes that have well-defined cytoplasms and nuclear structure. The sinusoidal morphology of normal liver tissue is also noticeable in this region. Additionally apparent in Figure 2(C) is the migratory action of inflammatory cells. At the 2-day mark, the inflammatory cells were found concentrated at the ablation boundary. However, at the 4-day mark, the inflammatory cells have moved from the ablation boundary into the necrotic zone, an event that has left an area of cellular debris that is easily discernible by the lack of nuclei. The inflammatory zone, however, can be easily recognized by the dark stained nuclei of the monocytes, predominant cell types at this stage.[19] At the ablation boundary, a fibroblast zone does exist, although an obvious and well-defined fibrous capsule is still lacking. This observation is supported by Figure 2(D), in which MTC stains show the presence of a small amount of extracellular collagen deposition arranged in a random manner.

Eight days after ablation

The inflammatory response due to tissue injury has progressed to the chronic stage 8 days after RF ablation and millirod implantation, and the formation of an extensive fibrous capsule, along with the appearance of new blood vessels, was observed. As is evident in Figure 3(A), a tight, dense layer of granulation tissue, averaging 1 mm in thickness, has formed adjacent to the ablation boundary, an event confirmed by the light blue staining region in the MTC image of Figure 3(C). Close examination of the fibrous matrix encapsulating the ablation region

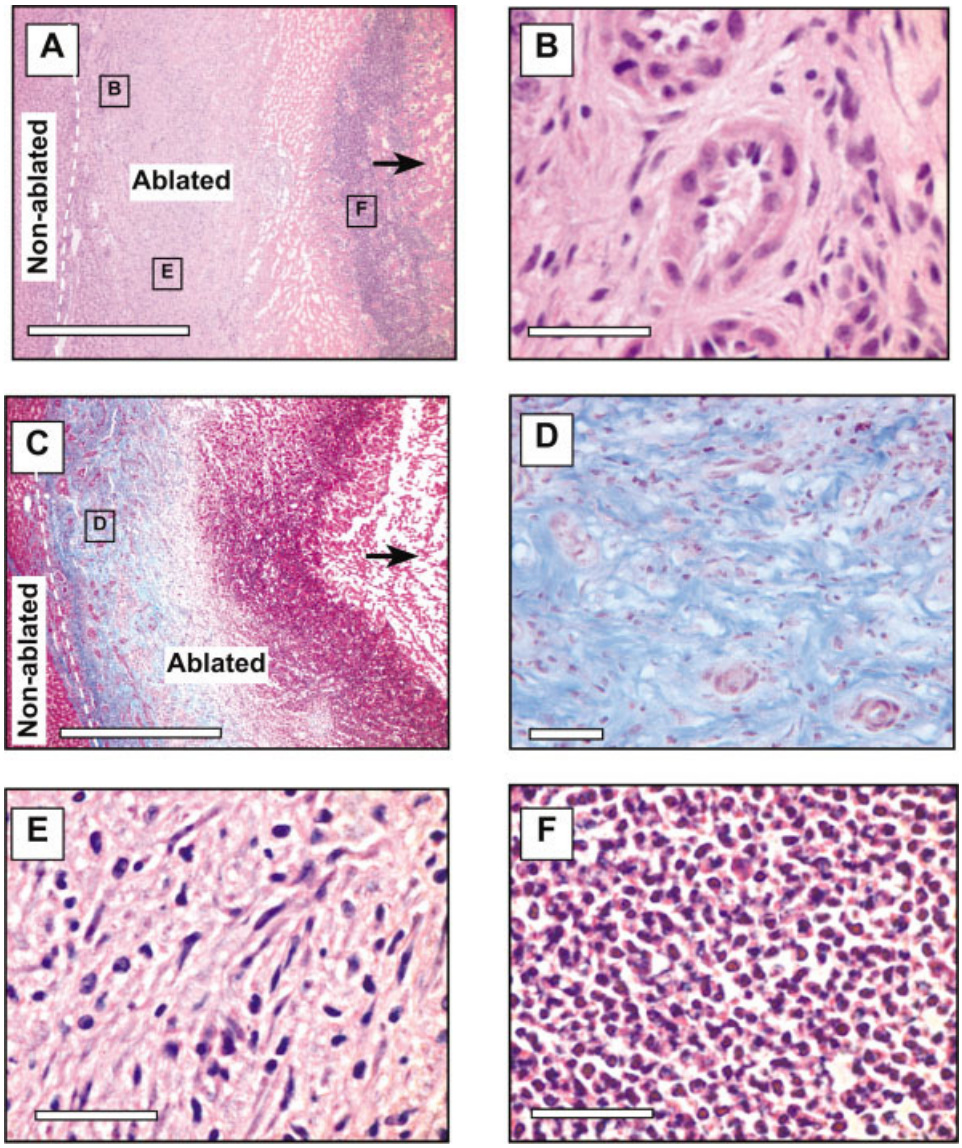

Figure 3. Liver tissue images 8 days after RF ablation and millirod implantation. (A) H&E image showing the distinct zones of ablation (original magnification 4×). (B) H&E magnification of new blood vessel formation (original magnification 60×). (C) MTC stain highlighting fibrous capsule formation in blue (original magnification 4×). (D) MTC magnification of fibroblasts within the fibrous capsule layer (original magnification 40×). (E) and (F) H&E magnifications of fibroblasts and inflammatory cells, respectively (original magnification 60×). The dashed lines in (A) and (C) delineate the ablation boundary, whereas the arrows in (A) and (C) point to the site of ablation probe insertion/millirod implantation. The scale bars in (A) and (C) represent 1 mm, whereas the scale bars in (B), (D), (E), and (F) represent 50 μm. [Color figure can be viewed in the online issue, which is available at www.interscience.wiley.com.]

[Fig. 3(B,D,E)] yields the presence of a high density of fibroblasts and a significant amount of collagen fibril deposition. Figure 3(A) also displays the presence of the five zones seen in samples collected 4 days after ablation. At the 8-day time point, the fibrous capsule layer has become broader than in the 4-day samples, and the zone of migrating inflammatory cells, amplified in Figure 3(F), has developed into a more massive aggregation that has come to include macrophages.

Apart from showing the extent of the dense collagen fibril layer, Figure 3(B) and (D) also shows neovascularization, or the formation of small new blood vessels, within the granulation tissue. As shown in the MTC-stained image [Fig. 3(D)], the endothelial tissues of the blood vessel wall are quite evident and stained red, whereas the surrounding fibrous capsule was stained light blue.

In two separate sets of control studies, the wound-healing response was examined after the implantation of doxorubicin-loaded millirods in nonablated livers, and the implantation of drug-free millirods in ablated livers (data not shown). In the sets of experiments conducted involving the implantation of

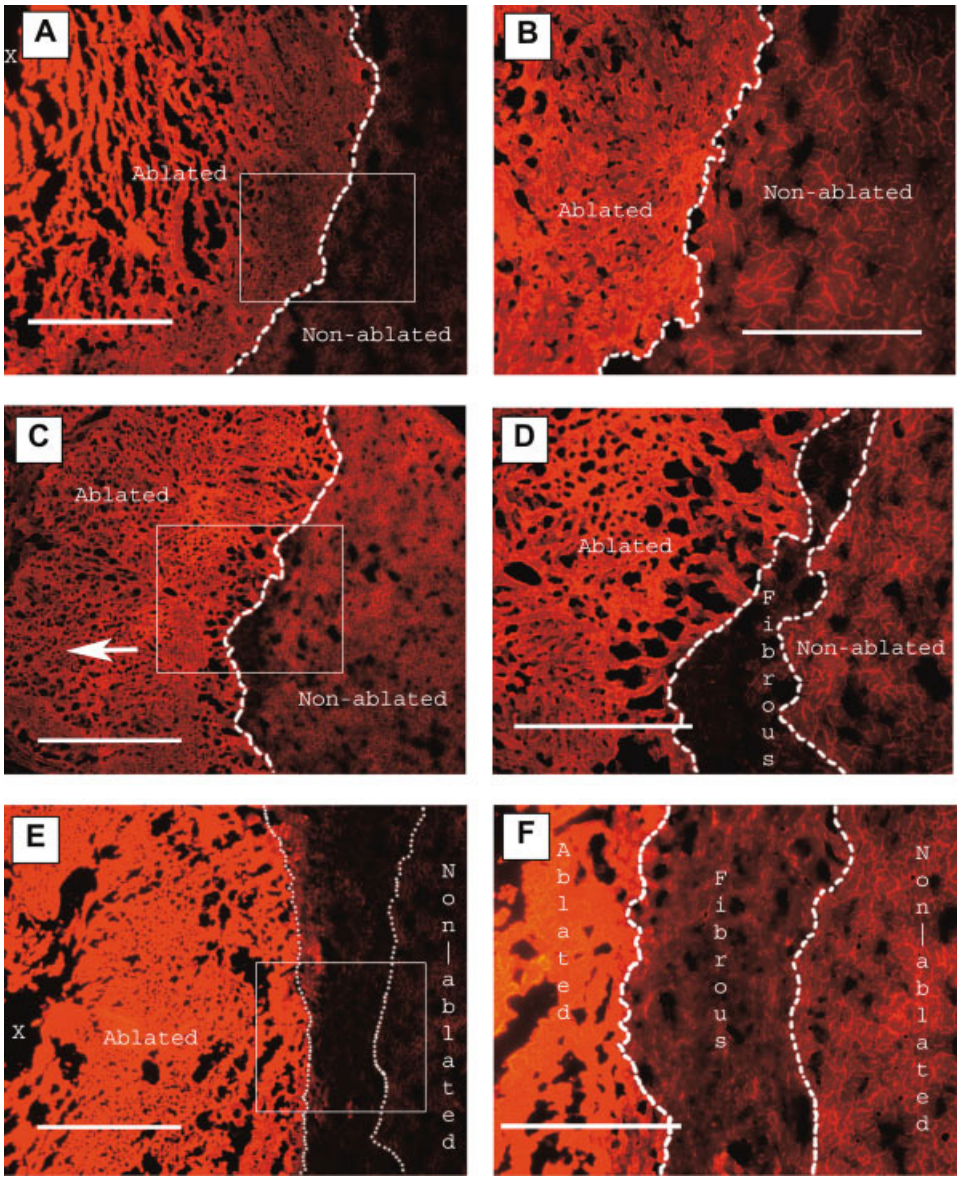

Figure 4. Fluorescence microscopy images of liver samples at various time points. (A), (C), and (E) Liver samples after RF ablation and millirod implantation at 2, 4, and 8 days, respectively (original magnification 4×). The boxed areas in (A), (C), and (E) are presented at higher magnifications (original magnification 10×) in figures (B), (D), and (F), respectively. The arrows point in the direction of the ablation probe insertion/millirod implantation site, with the letter X marking the site. The scale bars in (A), (C), and (E) are 1 mm, whereas the scale bars in (B), (D), and (F) are 0.5 mm. [Color figure can be viewed in the online issue, which is available at www.interscience.wiley.com.]

doxorubicin-loaded millirods in nonablated livers, the same wound-healing processes such as inflammatory cell migration and fibrous capsule formation were observed. However, the location of the fibrous capsule was localized around the site of implant, due mainly to the tissue injury resulting from puncturing the liver and from the presence of a foreign material. When drug-free control millirods were implanted in ablated livers, the five distinct zones presented above were readily identifiable, and a thick fibrous capsule engulfing the ablation region was observed after 8 days.

Doxorubicin distribution analysis

Fluorescence microscopy analysis: A qualitative approach

Figure 4 consists of fluorescence microscopy images obtained 2, 4, and 8 days after RF ablation, which provide insightful qualitative information on the effect of the fibrous capsule on doxorubicin distribution in RF-ablated livers. Although no morphological or nuclear detail can be discerned in these images, certain

features such as the millirod implantation site, the porous necrotic core, and the nonablated region with an intact sinusoidal network can be perceived. In Figure 4(A), a greater concentration of doxorubicin can be seen closer to the millirod implantation site 2 days after ablation, with the intensity waning throughout the necrotic core as it reaches the boundary. The magnification of the 2-day sample presented in Figure 4(B) allows for the appreciation of a sharp distinction between the ablated and nonablated regions; a higher concentration is shown to be localized within the necrotic core, with trace amounts of intensity appearing within sinusoids in the nonablated region.

Figure 4(C) and (D) shows fluorescence microscopy images of a liver sample 4 days after RF ablation. According to the histological findings presented in Figure 2(C) and (D), fibroblast activity occurs at this stage of the wound-healing response, as well as the early onset of collagen deposition, which will eventually yield a fibrous capsule adjacent to the ablation boundary. Figure 4(C) and (D) shows the presence of a dark, discontinuous region between the ablated and nonablated zones, a region with minimal to hardly any fluorescence intensity. Given its location, discontinuity, and lack of doxorubicin concentration, the zone labeled "fibrous" in Figure 4(D) is highly analogous to the fibroblast zone, and is assumed to be the early stages of fibrous capsule formation.

As shown in Figure 3, a dense and clearly defined fibrous capsule was shown to appear at the 8th day time point. Figure 4(E) shows the presence of a more extensive and well developed layer, the fibrous capsule, separating the ablated and nonablated regions, ranging from 0.5 to 1 mm in width. Of significant importance in the figure is the stark increase in doxorubicin concentration confined within the ablated region, a fluorescence intensity found to be in sharp contrast to the images obtained for the 2- and 4-day time points. The fibrous layer, better appreciated in magnification in Figure 4(F), shows low doxorubicin retention when compared with the adjacent ablated and nonablated regions.

Fluorescence imaging analysis: A quantitative approach

Fluorescence microscopy analysis provides a qualitative description of the doxorubicin distribution in a local region such as the ablation boundary. However, because of the potential photo bleaching effect, this method cannot provide reliable quantitative information on drug distribution in ablated and nonablated liver tissue. Instead, a fluorescence imaging method was used to obtain the quantitative macroscopic concentration–distance relationships for doxorubicin.

Figure 5 shows the doxorubicin concentration-versus-distance profiles for the 4- and 8-day time points. Although a slight increase in the doxorubicin concentration exists at the 4-day time point, the concentration is shown to decrease gradually with increasing distance from the millirod implant [Fig. 5(A)]. The figure inset in 5(A), a representative TIFF image whose fluorescence intensity has been converted to doxorubicin concentration using MatLab, qualitatively supports the general trend of the 4-day data, showing a slight accumulation of doxorubicin close to the millirod implantation site, with the concentration steadily decreasing at distances farther away from the implant. In Figure 5(B), the experimental data display a heightened doxorubicin concentration within the ablated region. The concentration remains roughly stable between 700 and 750 μg/g for a distance of 1 mm away from the millirod tissue interface, with concentration

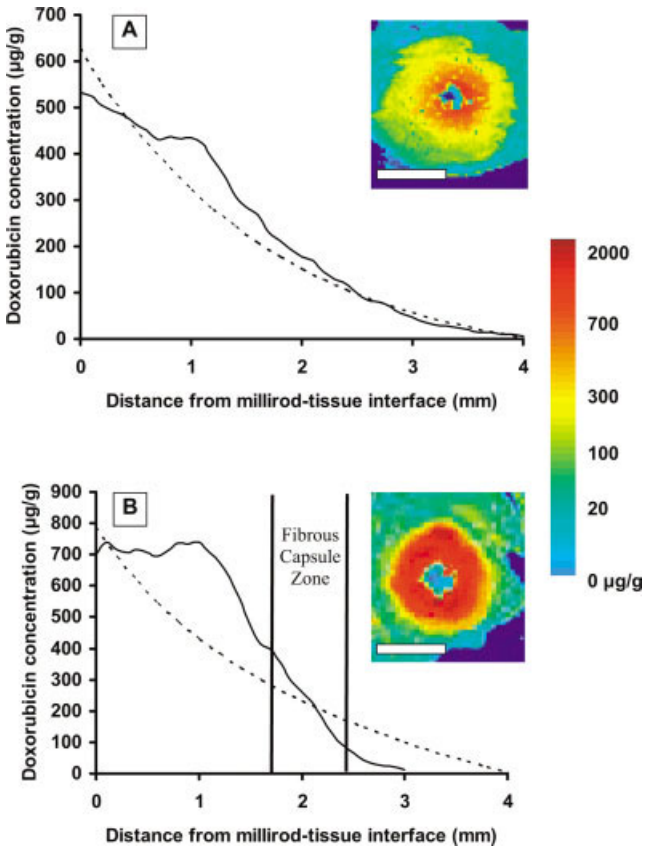

Figure 5. Doxorubicin concentration distribution in ablated liver tissues 4 days (A) and 8 days (B) after RF ablation and millirod implantation. The solid lines represent the experimental data obtained from fluorescence imaging analysis. The dashed lines represent the computer-predicted concentration–distance curves, using the following values for the constants D_a^*, D_n^*, γ^*: 1.1×10^{-7} cm^2s^{-1}, 6.7×10^{-7} cm^2s^{-1}, 9.6×10^{-4} s^{-1}, respectively. The bars in (B) represent the fibrous capsule zone. The figure insets represent fluorescent images of liver samples. The scale bars in the insets represent 5 mm. The color bar represents doxorubicin concentration. [Color figure can be viewed in the online issue, which is available at www.interscience.wiley.com.]

decreasing gradually upon the presence of the fibrous capsule and the nonablated region. The respective figure inset depicts the elevated doxorubicin concentration within the ablated region, an elevation that can best be explained by the invariant nature of ablated liver tissue, which at the 8-day time point has yielded a thicker encapsulating fibrous capsule.

Mathematical modeling of doxorubicin transport

Previously, we developed a mathematical model to quantitatively describe the drug transport processes in ablated and nonablated tissue.[15] The mathematical model in its present form assumes that there is a coexistence of drug in the free and bound forms in both ablated and nonablated regions, and that free drug concentration distribution in ablated tissue changes by diffusion and drug binding, and not by perfusion or metabolism. In nonablated tissue, drug will be lost because of perfusion and/or metabolism in addition to diffusion and binding processes. Based on the above transport processes, we developed steady-state concentration distributions in both regions:

$$C_a = \frac{r_p}{D_a^*} J \cdot \ln\left(\frac{r_s}{r}\right) + C_s \quad (1)$$

$$C_n = C_s \frac{K_0(\beta r)}{K_0(\beta r_s)} \quad (2)$$

Equation 1 describes the drug concentration in ablated tissue (C_a) as a function of radius (r) from the millirod implant (radius r_p). The release flux J represents the diffusion flux at the polymer–millirod interface ($r = r_p$),

$$J = -D_a^* \frac{\partial C_a}{\partial r} \quad (3)$$

The variable r_s is the distance from the millirod to the ablation boundary, and the term D_a^* is the apparent diffusivity in ablated tissue. Equation 2 describes the drug concentration in nonablated tissue (C_n) as a function of drug concentration (C_s) at the ablation boundary, with $K_0(\beta r)$ serving as a modified Bessel function of zero order. The parameters D_n^* and γ^*, included in the Bessel functions ($\beta = \sqrt{\gamma^*/D_n^*}$), are the apparent drug diffusivity in nonablated tissue and the apparent drug elimination coefficient, respectively. The apparent diffusivities D_a^*, D_n^*, and apparent drug elimination coefficient γ^* are assumed to be invariant of time, and were previously found to be 1.1×10^{-7} cm^2s^{-1}, 6.7×10^{-7} cm^2s^{-1}, and 9.6×10^{-4} s^{-1}, respectively, for doxorubicin.[16]

The model simulation curves for doxorubicin concentration versus distance are depicted in Figure 5. Figure 5(A) shows that the simulated model prediction curve correlates well with the experimental data obtained at the 4-day time point, corroborating the gradual decrease in drug concentration. However, in Figure 5(B), the model simulation curve does not adequately fit the experimental data at the 8-day time point, due primarily to the heightened doxorubicin concentration within the ablation boundary, itself an effect of the fibrous capsule.

DISCUSSION

The main purpose of this study was to examine the wound-healing response in RF-ablated rat livers and to evaluate whether the natural healing sequelae have an effect on drug distribution from the polymer millirod implant. The results from this study demonstrate that the ablated liver tissue is a time-variant system consisting of inhomogeneous zones spanning from the millirod implantation site to the outer periphery of the ablation boundary (Figs. 2 and 3).

Previously, we developed a mathematical model to describe the drug transport processes in ablated tissues. The model simplified the ablated liver tissue as a time-invariant system with two zones of homogeneous properties, the ablated and nonablated regions.[15,16] Within each region, the drug transport parameters (e.g., drug diffusivities and drug elimination coefficients) were assumed to be constant over time. Although this is a reasonable assumption to begin with, histology results in the current work demonstrate that the ablated liver tissue environment is much more complex, inhomogeneous in space and time. This premise is much more evident 4–8 days after ablation when extensive migration of inflammatory cells, proliferation of fibroblasts, formation of fibrous capsule, and neovascularization were observed.

Although the model predicts that the drug concentration should steadily decrease with increasing distance from the millirod at the 8-day time point, a significant deviation is observed in Figure 5(B). Fluorescence imaging analysis showed the appearance of a plateau in the drug concentration–distance curve, which demonstrates a pronounced increase in drug concentration within the ablated region. This increase in drug concentration correlates spatially with the location of the fibrous capsule [Fig. 5(B)] and is also supported by fluorescence microscopy results [Fig. 4(E,F)]. The excessive accumulation of connective tissue around the ablation boundary, consisting of highly organized and tightly packed collagen fibers, has led us to believe that this fibrous capsule acts as a barrier to drug transport. This barrier encapsulates the majority of the drug released from the millirod within the ablated region. These results agree fairly well with

the existing literature on drug transport deterrence with the emergence of collagenous tissue.[21–24]

In parallel with the formation of the fibrous capsule, neovascularization was also observed at the 8-day time point (Fig. 3). Previous studies showed that the implantation of millirods in nonablated livers had limited drug penetration because of the drug perfusion loss through sinusoidal vasculature.[15] Given that tumor recurrence was mostly observed at the ablation boundary,[25] neovascularization may present a challenge for local drug therapy. We hypothesize that the formation of new blood vessels may carry doxorubicin away from the ablation boundary, reducing drug exposure to residual cancer cells.

CONCLUSION

Results from this study illustrate that the wound-healing response after RF ablation has a significant impact on local drug pharmacokinetics. Perhaps the most significant finding is the obstructing nature of the fibrous capsule at the ablation boundary to drug transport. Current work is in progress to examine the incorporation of anti-inflammatory drugs (e.g., dexamethasone) within the polymer millirods with the hope of retarding the fibrous capsule formation, which in turn should facilitate drug delivery to the ablation boundary.

E. Blanco is grateful for the support of a National Institutes of Health minority supplement grant.

References

1. Seifert JK, Morris DL. Indicators of recurrence following cryotherapy for hepatic metastases from colorectal cancer. Br J Surg 1999;86:234–240.
2. Mascarenhas BA, Ravikumar TS. Experimental basis for hepatic cryotherapy. Semin Surg Oncol 1998;14:110–115.
3. Zhou XD, Tang ZY. Cryotherapy for primary liver cancer. Semin Surg Oncol 1998;14:171–174.
4. Malcolm AL, Ter Haar GR. Ablation of tissue volumes using high intensity focused ultrasound. Ultrasound Med Biol 1996; 22:659–669.
5. Rossi S, Garbagnati F, Rosa L, Azzaretti A, Belloni G, Quaretti P. Radiofrequency thermal ablation for treatment of hepatocellular carcinoma. Int J Clin Oncol 2002;7:225–235.
6. Wong SL, Edwards MJ, Chao C, Simpson D, McMasters KM. Radiofrequency ablation for unresectable hepatic tumors. Am J Surg 2001;182:552–557.
7. Wood BJ, Ramkaransingh JR, Fojo T, Walther MM, Libutti SK. Percutaneous tumor ablation with radiofrequency. Cancer 2002;94:443–451.
8. Curley SA, Izzo F. Radiofrequency ablation of primary and metastatic hepatic malignancies. Int J Clin Oncol 2002;7:72–81.
9. Kosari K, Gomes M, Hunter D, Hess DJ, Greeno E, Sielaff TD. Local, intrahepatic, and systemic recurrence patterns after radiofrequency ablation of hepatic malignancies. J Gastrointest Surg 2002;6:255–263.
10. Buscarini L, Buscarini E, Di Stasi M, Vallisa D, Quaretti P, Rocca A. Percutaneous radiofrequency ablation of small hepatocellular carcinoma: long-term results. Eur Radiol 2001;11: 914–921.
11. Harrison LE, Koneru B, Baramipour P, Fisher A, Barone A, Wilson D, Dela Torre A, Cho KC, Contractor D, Korogodsky M. Locoregional recurrences are frequent after radiofrequency ablation for hepatocellular carcinoma. J Am Coll Surg 2003;197: 759–764.
12. Qian F, Szymanski A, Gao J. Fabrication and characterization of controlled release poly(D,L-lactide-*co*-glycolide) millirods. J Biomed Mater Res 2001;55:512–522.
13. Qian F, Saidel G, Sutton D, Exner A, Gao J. Combined modeling and experimental approach for the development of dual-release polymer millirods. J Control Release 2002;83:427–435.
14. Qian F, Nasongkla N, Gao J. Membrane-encased polymer millirods for sustained release of 5-fluorouracil. J Biomed Mater Res 2002;61:203–211.
15. Qian F, Stowe N, Liu EH, Saidel GM, Gao J. Quantification of *in vivo* doxorubicin transport from PLGA millirods in thermoablated rat livers. J Control Release 2003;91:157–166.
16. Qian F, Stowe N, Gao J. Pharmacokinetic comparison of sustained and dual-release PLGA millirods in RF ablated rat livers. Pharm Res 2003. Forthcoming.
17. Imber G, Schwager RG, Guthrie RH, Gray GF. Fibrous capsule formation after subcutaneous implantation of synthetic materials in experimental animals. Plast Reconstr Surg 1974;54:183–186.
18. Coleman DL, King RN, Andrade JD. The foreign body reaction: a chronic inflammatory response. J Biomed Mater Res 1974;8: 199–211.
19. Anderson J. Mechanisms of inflammation and infection with implanted devices. Cardiovasc Pathol 1993;2:33S–41S.
20. Arturson G. Pathophysiology of the burn wound and pharmacological treatment. The Rudi Hermans lecture, 1995. Burns 1996;22:255–274.
21. Sharkawy AA, Klitzman B, Truskey GA, Reichert WM. Engineering the tissue which encapsulates subcutaneous implants. I. Diffusion properties. J Biomed Mater Res 1997;37:401–412.
22. Anderson JM, Niven H, Pelagalli J, Olanoff LS, Jones RD. The role of the fibrous capsule in the function of implanted drug–polymer sustained release systems. J Biomed Mater Res 1981; 15:889–902.
23. Wood RC, LeCluyse EL, Fix JA. Assessment of a model for measuring drug diffusion through implant-generated fibrous capsule membranes. Biomaterials 1995;16:957–959.
24. Poli G. Pathogenesis of liver fibrosis: role of oxidative stress. Mol Aspects Med 2000;21:49–98.
25. Komorizono Y, Oketani M, Sako K, Yamasaki N, Shibatou T, Maeda M, Kohara K, Shigenobu S, Ishibashi K, Arima T. Risk factors for local recurrence of small hepatocellular carcinoma tumors after a single session, single application of percutaneous radiofrequency ablation. Cancer 2003;97:1253–1262.